Robust quantum state transfer with topologically protected nodes

Yanlong Chang [ORCID], JiaoJiao Xue, Yuxiang Han [ORCID], Xiaoli Wang,[*] and Hongrong Li [ORCID][†]

School of Physics, Xi'an Jiaotong University, Xi'an 710049, China

Robust quantum state transfer (QST) is the foundation for information exchange among nodes in quantum networks. In this paper, we propose a robust QST protocol that utilizes topological edge modes in the qubit chains to encode (decode) quantum states (flying qubits). By employing qubits with tunable couplings, we construct Su-Schrieffer-Heeger (SSH) chains as the nodes of a quantum network. The end qubit of each SSH chain is dissipatively coupled to a chiral waveguide, and the dissipative strength is a constant. We refer to the SSH chain with a dissipation channel at the end qubit as the non-Hermitian SSH chain. Comparing the symmetry and energy spectra of the non-Hermitian SSH chain with those of the SSH chain, our analysis reveals that the dissipative dynamics of the topological edge state in the non-Hermitian SSH chain are governed by its imaginary spectra. The edge mode with the imaginary spectrum can be used to encode (decode) quantum states (flying qubits), thereby enabling robust QST between two remote mirrored non-Hermitian SSH chains. Our numerical simulations demonstrate that high-fidelity QST can be achieved even in the presence of coupling errors. Furthermore, we extend our analysis to consider QST in imperfect chiral waveguides, providing insights into the robustness of our protocol under realistic conditions. Our discussion is applicable to various quantum platforms and holds significant implications for constructing large-scale quantum networks.

I. INTRODUCTION

The quantum network is the cornerstone for large-scale quantum information processing [1–3]. The quantum state transfer (QST) between two nodes represents the basic unit of a quantum network. Many constructive QST solutions have been explored over the past few decades [4–14]. These protocols can be divided into two categories. The first type of protocols encode the quantum state into a flying qubit using a specialized dissipation function at the first node. Subsequently, the flying qubit is decoded back into a quantum state by reversing the dissipation function at the second node [15–20]. These protocols use chiral waveguides as channels, which greatly facilitate QST over long distances. Unfortunately, these protocols are sensitive to errors in tunable parameters, and noise in the waveguide also affects the fidelity of the QST. The second type of protocols have been developed to address these challenges by employing spin chains and spin-wave engineering, resulting in high-fidelity QST [21–23]. However, it is important to note that these protocols currently have technical limitations that restrict their applicability to short-distance QST. As a result, achieving high-fidelity QST over long distances remains a challenge.

The inherent resistance to disorder in topology has garnered significant attention [24–29], which has resulted in the integration of the concept of topology into various quantum platforms and research directions [26,30–34]. Topological quantum computation can be achieved through the utilization of non-Abelian arbitrary braided operations, which is one of the prominent approaches for realizing large-scale quantum computers [35,36]. A topologically protected laser can also be implemented using edge modes [37–39]. Furthermore, for the second type of QST protocols, by constructing generalized one-dimensional or two-dimensional topological systems, it is possible to achieve short-distance robust QST for tunable parameters and defects [12,40–44]. However, the research field of the first type of long-distance QST protected by topology is still a blank.

Inspired by Ref. [12], we present here an experimentally feasible protocol for robust long-distance QST utilizing non-Hermitian Su-Schrieffer-Heeger (SSH) chains as nodes, which encode (decode) quantum states (flying qubits) in topological edge modes. We first study the symmetry and dynamic properties of non-Hermitian SSH chains. The imaginary spectrum changes with the evolution of the edge state from the left edge mode to the right edge mode. In other words, the effective dissipation strength of the edge state can be changed by tuning the coupling parameters. Therefore we can encode (decode) the quantum state (flying qubit) to the flying qubit (quantum state) by adiabatic tuning of edge states, which exhibits robustness in the presence of coupling errors. We subsequently investigate QST between two non-Hermitian SSH chains as nodes. This transfer is achieved by implementing a time-reversal process, whereby the flying qubit encoded at node 1 is decoded at node 2. Through numerical simulations, we demonstrate the robustness of the QST protocol in the presence of errors in tunable coupling parameters and fixed dissipation strength. Imperfect chiral waveguides can also impact the fidelity of QST. However, when the distance between nodes is an integral multiple of the wavelength, high-fidelity
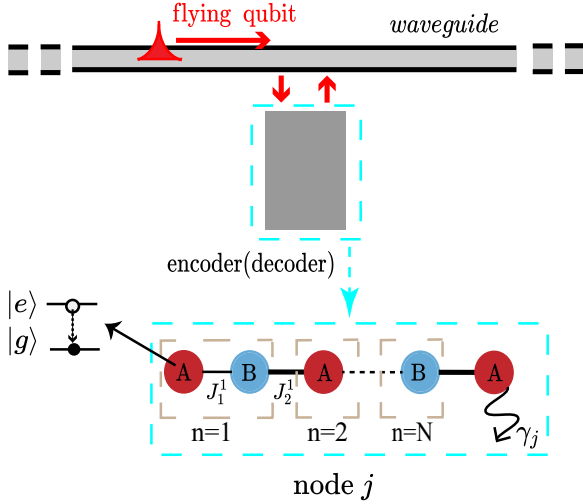
FIG. 1. A non-Hermitian SSH chain, serving as a node in a quantum network, has the capability to encode (decode) quantum states (flying qubits) on its topological edge state.

QST can still be achieved. Our results demonstrate that the encoding (decoding) of the quantum state (flying qubit) is protected by topology, specifically the finite band gap between the bulk and edge states of the non-Hermitian SSH chain. Thus we show that high-fidelity QST can still be achieved even in the presence of relatively large coupling parameter errors. This protocol can be implemented on qubit systems, including optomechanical systems, trapped ions, and superconducting circuits.

This paper is organized as follows. In Sec. II, we introduce the non-Hermitian SSH chains as the nodes of a quantum network and study their symmetry, energy spectrum, and dynamic properties. In Sec. III, we demonstrate the QST between two non-Hermitian SSH chains and conduct numerical simulations to investigate the impact of coupling errors and imperfect chiral waveguides on the fidelity of the transfer. In Sec. IV, we summarize the results.

II. NON-HERMITIC SSH CHAINS

In our QST protocol, we employ the non-Hermitian SSH chains as the nodes. Considering the equivalence of all nodes in the quantum network, in Fig. 1 we only show node j. The node is a non-Hermitian SSH chain composed of $N + 1$ A-type qubits and N B-type qubits, with the quantum state dissipating into the waveguide through the end qubit. Both the storage and reading of quantum states take place at the first qubit. The Hamiltonian of node j is

$$H_j = \sum_{n=1}^{N} \left(J_1^j \sigma_{A_{j,n}}^+ \sigma_{B_{j,n}}^- + J_2^j \sigma_{A_{j,n+1}}^+ \sigma_{B_{j,n}}^- + \text{H.c.} \right)$$
$$+ i\gamma_j \sigma_{A_{j,N+1}}^+ \sigma_{A_{j,N+1}}^-, \qquad (1)$$

where $\sigma_{A_{j,n}}^+ = |e\rangle_{A_{j,n}} \langle g|$ ($\sigma_{B_{j,n}}^+ = |e\rangle_{B_{j,n}} \langle g|$) is the Pauli operator of the nth A-type (B-type) qubit and J_1^j and J_2^j represent the intracell (thin lines) and intercell (bold lines) coupling strengths, respectively. The dissipative coupling strength between the

end qubit and the waveguide is γ_j, which is a constant. The first term of the Hamiltonian describes the standard SSH chain, and the second term describes the gain or dissipation.

In the single-excitation subspace, the wave function of node j can be written as

$$|\psi\rangle_j = \sum_{n=1}^{N+1} (\alpha_{j,n} \sigma_{A_{j,n}}^+ + \beta_{j,n} \sigma_{B_{j,n}}^+)|G\rangle_j, \qquad (2)$$

where $|G\rangle_j = |gg \cdots g\rangle_j$ is the ground state and $\beta_{j,N+1} = 0$.

Next, we will proceed with a comprehensive analysis of the edge states and dynamic characteristics exhibited by non-Hermitian SSH chains.

A. Symmetry and the energy spectrum

Symmetries such as time-reversal symmetry (TRS), particle-hole symmetry (PHS), and chiral symmetry (CS), are crucial in the topological phases; they determine the classification of topological phases. The standard SSH chains satisfy chiral symmetry. We define $\mathcal{T}$, $\mathcal{P}$, and $\mathcal{C} = \mathcal{TP}$ as the time-reversal operator, the particle-hole operator, and the chiral operator, respectively, where $\mathcal{T}$ and $\mathcal{P}$ are antiunitary and $\mathcal{C}$ is unitary. In the case of discrete lattice points, the operators $\mathcal{T}$, $\mathcal{P}$, and $\mathcal{C}$ act as $\mathcal{T}i\mathcal{T}^{-1} = -i$, $\mathcal{P}i\mathcal{P}^{-1} = i$, $\mathcal{C}i\mathcal{C}^{-1} = -i$. For the non-Hermitian SSH chain presented in this paper, we can obtain

$$\mathcal{T}H_{j,\text{SSH}}\mathcal{T}^{-1} = H_{j,\text{SSH}}, \quad \mathcal{P}H_{j,\text{SSH}}\mathcal{P}^{-1} = -H_{j,\text{SSH}},$$
$$\mathcal{T}H_{j,P}\mathcal{T}^{-1} = -H_{j,P}, \quad \mathcal{P}H_{j,P}\mathcal{P}^{-1} = H_{j,P},$$
$$\mathcal{C}H_{j,\text{SSH}}\mathcal{C}^{-1} = -H_{j,\text{SSH}}, \quad \mathcal{C}H_j\mathcal{C}^{-1} = -H_j, \qquad (3)$$

where $H_{j,\text{SSH}}$ is the Hamiltonian of the SSH chain and $H_{j,P} = i\gamma_j \sigma_{A_{j,N+1}}^+ \sigma_{A_{j,N+1}}^-$ is the non-Hermitian term. The non-Hermitian SSH chain satisfies chiral symmetry.

As shown in Fig. 2, we numerically simulate the energy spectrum of the non-Hermitian SSH chain with open boundary conditions, where $N = 2$, $J_1^j = J_0(1 - \cos\theta)$, and $J_1^j = J_0(1 + \cos\theta)$. Here, $J_0 = 5$ MHz is the coupling constant. As depicted in Fig. 2(a), the real spectrum of non-Hermitian SSH chains remains the same as that of SSH chains ($\gamma_j = 0$ MHz), irrespective of whether they exhibit gain ($\gamma_j = 1$ MHz) or dissipative ($\gamma_j = -1$ MHz) behavior. Figure 2(b) shows the complex spectrum of the SSH chain ($\gamma_j = 0$ MHz). Taking the non-Hermitian term $i\gamma_j$ into account, we expect it to have an impact on the energy spectrum of the SSH model. In Fig. 2(c), there is a base energy in the full complex energy spectrum that does not contact other energy bands. This indicates the existence of an edge state in the non-Hermitic SSH chain with $\gamma_j = -1$ MHz [45,46]. The presence of chiral symmetry in the system imposes a requirement that the base energy must lie on the imaginary axis (Re$E_{j,0} = 0$), accompanied by the appearance of energy eigenvalue pairs ($E_j, -E_j^*$) [46]. This requirement is strongly supported by the complex energy spectrum analysis. It can be seen that within a period, the imaginary energy will change from 0 to -1 and then from -1 to 0 in Fig. 2(c), which is easy to understand. As is known to all, the edge state is concentrated in the left end of the SSH chain when $-\pi/2 < \theta < \pi/2$ and in the right end when $\pi/2 < \theta < 3\pi/2$. The distribution of the edge state in the
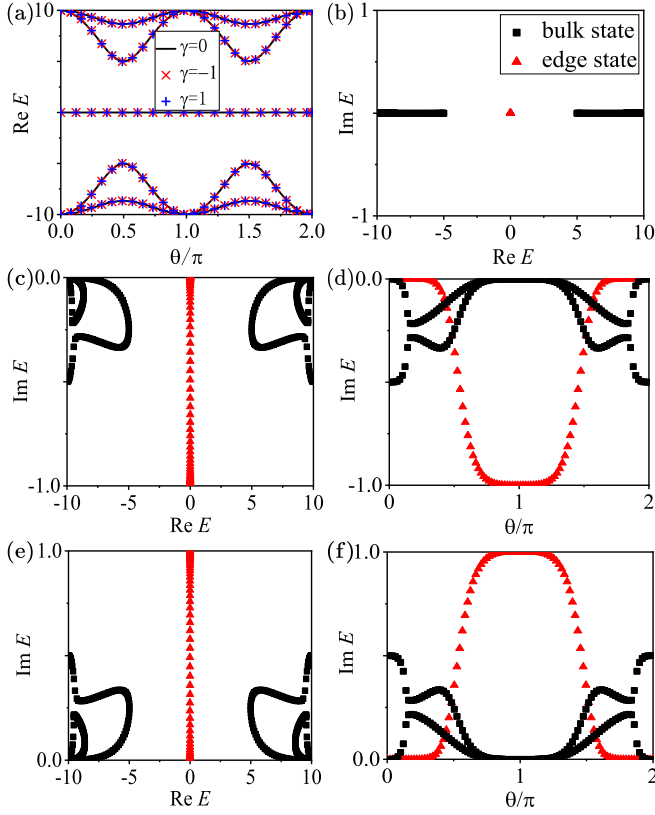
FIG. 2. Energy spectrum of a non-Hermitian SSH chain. (a) The real spectrum of the non-Hermitian SSH chain ($\gamma_j = -1$ MHz and $\gamma_j = 1$ MHz) almost coincides with the real spectrum of the SSH chain ($\gamma_j = 0$ MHz). (b) The complex spectrum of the SSH chain. (c) and (d) For $\gamma_j = -1$ MHz, the complex spectrum and the imaginary spectrum of the non-Hermitian SSH chain, respectively. (e) and (f) The complex spectrogram and imaginary spectrogram for $\gamma_j = 1$ MHz, respectively. In [(b)–(f)], red triangles represent topological edge states, and black squares represent bulk states.

B. Dynamics and robustness

In this section, we will analyze the dynamics of non-Hermitian SSH chains and their robustness in the presence

non-Hermitian SSH chain exhibits a similarity to that in the SSH chain. However, the presence of a dissipative channel at the end qubit results in a relatively smaller effective dissipation strength (imaginary energy) for the left-end-concentrated edge state. Conversely, when the edge state is concentrated on the right end, the effective dissipation strength (imaginary energy) becomes larger. In particular, at $\theta = 0$ and $\theta = \pi$, the imaginary energy of the edge state becomes 0 or $i\gamma_j$, respectively. The energy spectrum of the non-Hermitian SSH chain with gain is illustrated in Figs. 2(e) and 2(f). Comparing Figs. 2(e) and 2(f) with Figs. 2(c) and 2(d), we find that the situation is essentially the same for both gain and dissipation, but the topological edge state always exhibits gain behavior. Figure 2 illustrates that non-Hermitian SSH chains have topological edge states similar to those of SSH chains. Specifically, the edge states in non-Hermitian SSH chains can exhibit gain or dissipative behavior, and their strength is tunable.

of coupling errors. We set the coupling strengths $J_1^j = J_0(1 - \cos(\omega t))$ and $J_2^j = J_0(1 + \cos(\omega t))$, where ω is the adjustment frequency and t is time. The Hamiltonian $H_j(t)$ is time dependent. Here we investigate the evolution of the wave function under adiabatic changes in the Hamiltonian. The instantaneous eigenequation of node j can be written as

$$H_j(t)|E_{j,n}(t)\rangle = E_{j,n}(t)|E_{j,n}(t)\rangle, \tag{4}$$

where $|E_{j,n}(t)\rangle$ is the instantaneous eigenstate and $E_{j,n}(t)$ is the instantaneous eigenenergy. Therefore the wave function at any time can be written in the following form:

$$|\psi(t)\rangle_j = \sum_n a_{j,n}(t)e^{-i\int_0^t E_{j,n}(t')dt'}|E_{j,n}(t)\rangle. \tag{5}$$

Substituting Eq. (5) into the Schrödinger equation, and considering the adiabatic condition, we can obtain

$$a_{j,n}(t) = e^{-\int_0^t \langle E_{j,n}(t')|\partial_{t'}|E_{j,n}(t')\rangle dt'}a_n(0). \tag{6}$$

Our focus is on the edge eigenstate $|E_{j,0}(t)\rangle$ of the non-Hermitian SSH chain. We require the initial state to be set as the edge eigenstate. In this case, $a_{j,0}(0) = 1$, and the time-dependent wave function is

$$|\psi(t)\rangle_j = e^{i\varphi_{j,1}}e^{-i\varphi_{j,2}}|E_{j,0}(t)\rangle, \tag{7}$$

where $\varphi_{j,1} = i\int_0^t \langle E_{j,n}(t')|\partial_{t'}|E_{j,n}(t')\rangle dt'$ is the adiabatic phase and $\varphi_{j,2} = \int_0^t E_{j,n}(t')dt'$ is the dynamic phase.

Next, we investigate the eigenenergy of the edge states. By substituting Eq. (2) into the energy eigenequation corresponding to the edge state, we can derive the following expression:

$$E_{j,0}\alpha_{j,n} = J_1^j\beta_{j,n} + J_2\beta_{j,n-1} \quad (1 \leqslant n \leqslant N), \tag{8}$$

$$E_{j,0}\alpha_{j,N+1} = J_2^j\beta_{j,N} + i\gamma_j\alpha_{j,N+1}, \tag{9}$$

$$E_{j,0}\beta_{j,n} = J_1^j\alpha_{j,n} + J_2^j\alpha_{j,n+1} \quad (1 \leqslant n \leqslant N). \tag{10}$$

Rewriting Eqs. (8)–(10), we can obtain

$$E_{j,0}|\alpha_{j,n}|^2 = J_1^j\beta_{j,n}\alpha_{j,n}^* + J_2^j\beta_{j,n-1}\alpha_{j,n}^* \quad (1 \leqslant n \leqslant N), \tag{11}$$

$$E_{j,0}|\alpha_{j,N+1}|^2 = J_2^j\beta_{j,N}\alpha_{j,N+1}^* + i\gamma_j|\alpha_{j,N+1}|^2, \tag{12}$$

$$E_{j,0}|\beta_{j,n}|^2 = J_1^j\alpha_{j,n}\beta_{j,n}^* + J_2^j\alpha_{j,n+1}\beta_{j,n}^* \quad (1 \leqslant n \leqslant N), \tag{13}$$

where $\beta_{j,0} = 0$. In Sec. II A, we proved that the eigenenergy $E_{j,0}$ of the edge state is purely imaginary. We sum both sides of Eqs. (11)–(13) and get the energy expression for the edge state as

$$E_{j,0} = i\gamma_j|\alpha_{j,N+1}|^2. \tag{14}$$

As expected, the edge state energy of a non-Hermitian SSH chain is an imaginary number. Its magnitude is determined by the product of the gain or dissipative strength γ_j and the density of states of the qubit where the dissipative channel exists. When time t is relatively small, the edge state of the non-Hermitian SSH chain is predominantly localized at the left end. Consequently, the amplitude at the rightmost qubit is very small, resulting in a relatively low eigenenergy. However, as t increases, the edge state becomes localized at the right end

of the chain. The amplitude at the rightmost qubit gradually increases, leading to an increase in the eigenenergy. Indeed, since the eigenenergy of the edge state is imaginary, it can be referred to as the effective gain or dissipation strength of the edge state. By substituting the eigenenergy of the edge state into Eq. (7), we can obtain

$$\varphi_{j,2} = \int_0^t E_{j,n}(t')dt' = \int_0^t i\gamma_j|\alpha_{j,N+1}|^2 dt'. \quad (15)$$

The dynamic phase $\varphi_{j,2}$ can be viewed as a gain or dissipation factor, which is indirectly controlled by the couplings J_1^j and J_2^j. In addition, if the integration interval is $[0, 2\pi/\omega]$, the adiabatic phase $\varphi_{j,1} = i\int_0^t \langle E_{j,0}(t')|\partial_{t'}|E_{j,0}(t')\rangle dt'$ is also the topological phase of a non-Hermitian SSH chain, i.e., $\varphi_{j,1} = \pi$. Therefore, through the adiabatic tuning of coupling parameters, the edge state of a non-Hermitian SSH chain accumulates a phase factor and undergoes spontaneous gain or dissipation.

The edge states of non-Hermitian SSH chains exhibit antidisorder properties. The process of encoding quantum states into flying qubits at nodes involves controlling the effective dissipation strength to construct the desired shape of the flying qubits $\sqrt{\gamma_j}\alpha_{j,N+1}$. In our protocol, the effective dissipative strength of the topological edge state is controlled through the coupling parameters. Therefore any errors in encoding (decoding) the quantum state (flying qubits) on the edge mode are attributed to the tunable coupling strength between the qubits, which can be described as the following Hamiltonian:

$$\hat{H}_{\text{error}}^j = \sum_n^N \left(\delta J_1^j \sigma_{A_{j,n}}^+ \sigma_{B_{j,n}}^- + \delta J_2^j \sigma_{B_{j,n}}^+ \sigma_{A_{j,n+1}}^-\right) + \text{H.c.,} \quad (16)$$

where $\delta J_{1/2}^j = gJ_0\delta_{1/2,n}^j$, g is the imperfection strength, and $\delta_{1,n}^j$ ($\delta_{2,n}^j$) $\in [-0.5, 0.5]$ is the random number of the coupling strength error between the nth B-type qubit and the nth [$(n+1)$th] A-type qubit on the non-Hermitian SSH chain at node j.

In Fig. 3, we investigate the evolution of an initial state $|\psi(t=0)\rangle_j = (|gg\cdots g\rangle_j + |eg\cdots g\rangle_j)/\sqrt{2}$ under couplings with errors and compare the resulting changes in the flying qubits, where $J_0 = 5$ MHz, $\omega = 0.1$ MHz, and $\gamma_j = 0.6$ MHz. It is evident that when the coupling parameter errors are not substantial, the shape of the flying qubit closely resembles that of the flying qubit under ideal parameters.

III. QUANTUM STATE TRANSFER

In this section, we will present a QST protocol using the non-Hermitian SSH chains as quantum network nodes. Our objective is to transfer any superposition state $c_g|g\rangle_1 + c_e|e\rangle_1$ located at node 1 to node 2:

$$(c_g|G\rangle_1 + c_e|eg\cdots g\rangle_1)|G\rangle_2 \otimes |\text{vac}\rangle$$
$$\rightarrow |G\rangle_1(c_g|G\rangle_2 + c_e|eg\cdots g\rangle_2) \otimes |\text{vac}\rangle, \quad (17)$$

where $|G\rangle_1 = |gg\cdots g\rangle_1$ and $|G\rangle_2 = |gg\cdots g\rangle_2$ are the ground states of node 1 and node 2, respectively. The QST protocol is divided into three steps. We start by encoding the quantum state at node 1 onto the flying qubit. This encoding process occurs on the edge mode of the non-Hermitian SSH chain.
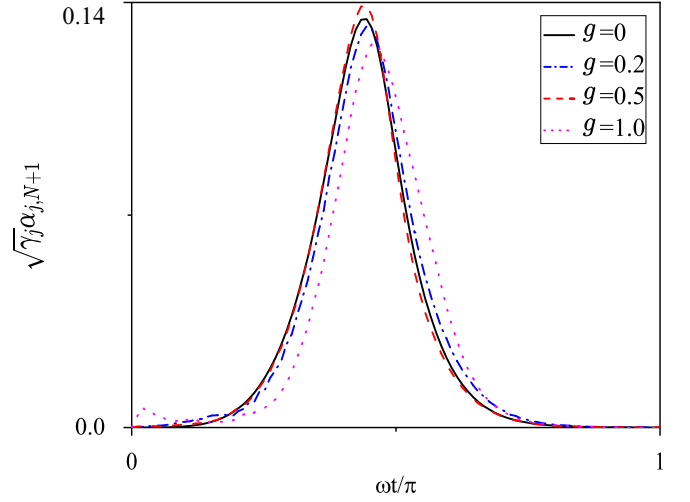

FIG. 3. The variation of the flight qubit under different coupling parameter errors. The imperfection strengths are $g = 0$ (solid black curve), $g = 0.2$ (dash-dotted blue curve), $g = 0.5$ (dashed red curve), and $g = 1.0$ (dotted magenta curve). We conducted ten numerical simulations for each value of imperfect strength and then calculated the average.

Subsequently, the flying qubit propagates through the chiral waveguide to node 2. Finally, at node 2, the flying qubit is decoded to retrieve the quantum state using the edge mode.

Next, we will demonstrate the QST between two non-Hermitian SSH chain nodes. Subsequently, we will analyze the impact of coupling errors and imperfect chiral waveguides on the fidelity of QST through numerical simulations.

A. Model

As shown in Fig. 4, we present a QST protocol between two nodes composed of non-Hermitian SSH chains. The two nodes are interconnected by a chiral waveguide, facilitating the transfer of quantum states between them. The system can be described by the Hamiltonian $\hat{H} = \sum_{j=1,2} \hat{H}_j + \hat{H}_I$, where $\hat{H}_j$ represents the Hamiltonian of node j and $\hat{H}_I$ represents the dissipative coupling between the nodes and the waveguide. The dissipative coupling strength γ_j is a constant.

In the waveguide, the modes are continuous, but for our analysis, we will consider the finite bandwidth $\mathcal{B}$ and the linear dispersion relationship around the qubit frequency ω_{eg}. In addition, we also assume that the decay rate γ_j is a constant over the bandwidth $\mathcal{B}$. The nodes are designed with a chiral light-matter interface with coupling to right-moving modes of the waveguide, and the interaction Hamiltonian can be expressed as

$$\hat{H}_I = i\sqrt{2\gamma_1}c_R^\dagger(t)\sigma_{A_{1,N+1}}^- + i\sqrt{2\gamma_2}c_R^\dagger(t-\tau)e^{i\phi_R}\sigma_{A_{2,N+1}}^- - \text{H.c.,} \quad (18)$$

where τ denotes the time delay of the propagation between the two nodes and $\phi_R = \omega_{eg}\tau$ is the propagation phase. Both τ and ϕ_R can be absorbed by redefining the time and phase of node 2. The quantum noise operators $c_R(t) = \frac{1}{2\pi}\int_\mathcal{B} d\omega c_R(\omega)e^{-i(\omega-\omega_{eg})t}$ satisfy $[c_R(t), c_R^\dagger(t')] =$
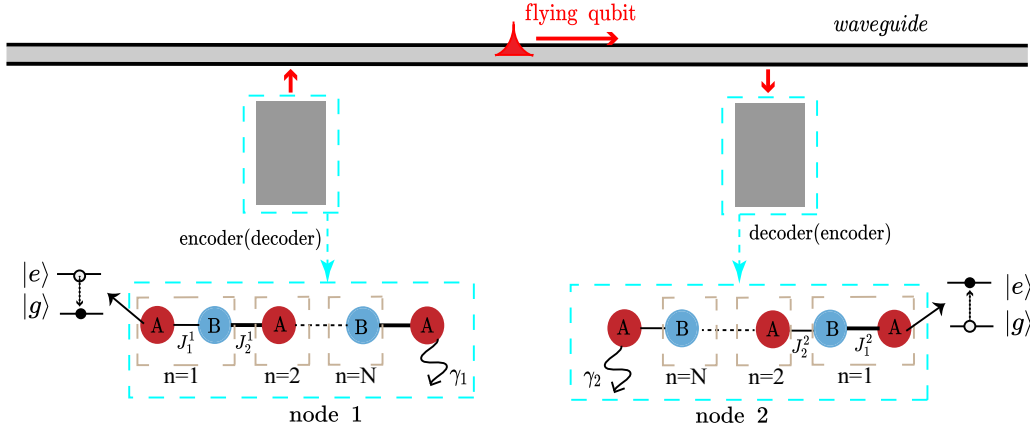
FIG. 4. QST between two nodes, where the chiral waveguide acts as a channel connecting the nodes. The non-Hermitian SSH chains act as nodes to encode (decode) quantum states (flying qubits) via topological edge modes.

$\delta(t - t')$. Here, $c_R(\omega)$ denotes the annihilation operators of the waveguide of right-moving modes.

Assuming a composite system composed of nodes and chiral waveguides, without additional dissipation channels, the evolution of the composite system can be described by the Schrödinger equation:

$$i\frac{d}{dt}|\Psi(t)\rangle = \hat{H}(t)|\Psi(t)\rangle, \tag{19}$$

where $|\Psi(t)\rangle$ is the wave function. Here, we only consider a single excited subspace, and $|n, T\rangle_j$ represents the base vector of the nth T-type $(T = A, B)$ qubit of node j. The amplitude at each qubit is $\alpha_{j,n} = {}_j \langle n, A|\Psi\rangle$ $(\beta_{j,n} = {}_j \langle n, B|\Psi\rangle)$, and $\psi_0 = \langle W|\Psi\rangle$ is the noise in the waveguide. The equations of motion of the qubits are $(\hbar = 1)$

$$i\dot{\alpha}_{j,n} = J_1^j \beta_{j,n} + J_2^j \beta_{j,n-1} \quad (1 \leqslant n \leqslant N), \tag{20}$$

$$i\dot{\beta}_{j,n} = J_1^j \alpha_{L,n} + J_2^j \alpha_{j,n+1} \quad (1 \leqslant n \leqslant N), \tag{21}$$

$$i\dot{\alpha}_{1,N+1} = J_2^1 \beta_{1,N} - i\gamma_1 \alpha_{1,N+1} - i\sqrt{2\gamma_1}\psi_0, \tag{22}$$

$$i\dot{\alpha}_{2,N+1} = J_1^2 \beta_{2,N} - i\gamma_2 \alpha_{2,N+1} \\ - i\sqrt{2\gamma_2}(\psi_0 + \sqrt{2\gamma_1}\alpha_{1,N+1}). \tag{23}$$

We assume that there is no noise in the waveguide, i.e., $\psi_0 = 0$, and the effective Hamiltonian corresponding to the system is

$$\hat{H}_{\text{eff}} = \sum_{j=1,2} \sum_{n=1}^{N} \left(J_1^j \sigma_{A_{j,n}}^+ \sigma_{B_{j,n}}^- + J_2^j \sigma_{B_{j,n}}^+ \sigma_{A_{j,n+1}}^- + \text{H.c.}\right) \\ - i\gamma_1 \sigma_{A_{1,N+1}}^+ \sigma_{A_{1,N+1}}^- - i\gamma_2 \sigma_{A_{2,N+1}}^+ \sigma_{A_{2,N+1}}^- \\ - 2i\sqrt{\gamma_1\gamma_2}\sigma_{A_{2,N+1}}^+ \sigma_{A_{1,N+1}}^-. \tag{24}$$

According to the effective Hamiltonian, we write the corresponding wave function of the effective system as

$$|\Psi_0(t)\rangle = \sum_{j=1,2} \sum_{n=1}^{N+1} (\alpha_{j,n}\sigma_{A_{j,n}}^+ + \beta_{j,n}\sigma_{B_{j,n}}^+)|G\rangle, \tag{25}$$

where $|G\rangle = |G\rangle_1 |G\rangle_2 = |gg\cdots g\rangle_1 |gg\cdots g\rangle_2$ is the ground state.

In order to achieve ideal QST, it is crucial to ensure that the effective system remains closed, meaning that no information leaks into the environment:

$$\frac{d}{dt}\langle\Psi_0(t)|\Psi_0(t)\rangle = i\langle\Psi_0(t)|(\hat{H}_{\text{eff}}^\dagger - \hat{H}_{\text{eff}})|\Psi_0(t)\rangle \\ = 0. \tag{26}$$

Substituting Eqs. (24) and (25) into Eq. (26), we get the following relationship:

$$-2\gamma_1|\alpha_{1,N+1}|^2 - 2\gamma_2|\alpha_{2,N+1}|^2 - 4\sqrt{\gamma_1\gamma_2}\alpha_{2,N+1}^*\alpha_{1,N+1} = 0. \tag{27}$$

Since the first two terms of the equation are real numbers, we can rewrite Eq. (27) as

$$-2|\sqrt{\gamma_1}\alpha_{1,N+1} + \sqrt{\gamma_1}\alpha_{2,N+1}|^2 = 0. \tag{28}$$

That is to say,

$$\alpha_{1,N+1} = -\eta\alpha_{2,N+1} \quad \left(\eta = \sqrt{\frac{\gamma_2}{\gamma_1}}\right). \tag{29}$$

This is the dark-state condition for ideal QST.

We then verify that the ideal QST is performed on the topological edge mode of two non-Hermitian SSH chains. By considering the energy eigenequation corresponding to the edge mode of the effective system, we can obtain

$$E_{1,0}|\alpha_{1,n}|^2 = J_1\beta_{1,n}\alpha_{1,n}^* + J_2\beta_{1,n-1}\alpha_{1,n}^* \quad (1 \leqslant n \leqslant N), \tag{30}$$

$$E_{1,0}|\alpha_{1,N+1}|^2 = J_2\beta_{1,N}\alpha_{1,N+1}^* - i\gamma|\alpha_{1,N+1}|^2, \tag{31}$$

$$E_{1,0}|\beta_{1,n}|^2 = J_1\alpha_{1,n}\beta_{1,n}^* + J_2\alpha_{1,n+1}\beta_{1,n}^* \quad (1 \leqslant n \leqslant N), \tag{32}$$

$$E_2, 0|\alpha_{2,n}|^2 = J_1\beta_{2,n}\alpha_{2,n}^* + J_2\beta_{2,n-1}\alpha_{2,n}^* \quad (1 \leqslant n \leqslant N), \tag{33}$$

$$E_{2,0}|\alpha_{2,N+1}|^2 = J_2\beta_{2,N}\alpha_{2,N+1}^* - i\gamma_2|\alpha_{2,N+1}|^2 \\ - 2i\sqrt{\gamma_1\gamma_2}\alpha_{1,N+1}\alpha_{2,N+1}^*, \tag{34}$$
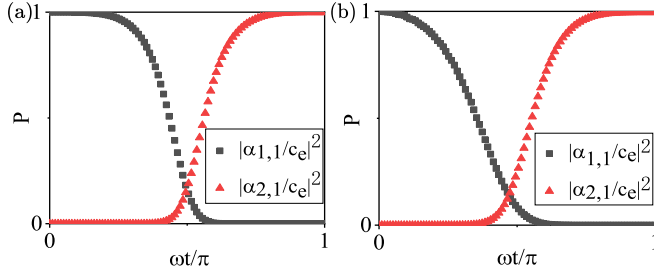
FIG. 5. The QST between two nodes. (a) The coupling parameters of the two nodes are in a time-reversal relationship with each other. The amplitude change of the first qubit on node 2 and the first qubit on node 1 also exhibits time inversion. (b) The coupling parameters of the two nodes are independent. The amplitude of the first qubit on node 1 gradually decreases to 0, while the amplitude of the first qubit on node 2 gradually increases to 1.

$$E_{2,0}|\beta_{2,n}|^2 = J_1\alpha_{2,n}\beta_{2,n}^* + J_2\alpha_{2,n+1}\beta_{2,n}^* \quad (1 \leqslant n \leqslant N), \quad (35)$$

where $E_{1,0}$ and $E_{2,0}$ are the eigenenergies at node 1 and node 2, respectively. In order to achieve an ideal QST, Eq. (29) must be satisfied. Substituting this condition into Eq. (34), we find that

$$E_2|\alpha_{2,N+1}|^2 = J_2\beta_{2,N}\alpha_{2,N+1}^* + i\gamma_2|\alpha_{2,N+1}|^2. \quad (36)$$

According to what we proved in the previous section, Eqs. (29)–(36) indicate that in order to achieve ideal QST, the quantum state must evolve on the edge states of the two non-Hermitian SSH chains.

By tuning coupling strengths, we can encode the quantum state at node 1 onto the flying qubit. Conversely, if we reverse the time, the flying qubit will be decoded, transferring the quantum state back to node 1. To achieve ideal QST, we assume that the process of decoding the flying qubit at node 2 is equivalent to time-reversing the process of encoding the quantum state at node 1. This assumption relies on the symmetry of the flying qubit's shape. Additionally, we obtain the coupling parameters of node 2 by performing time inversion on the coupling parameters of node 1. Returning to the setup of Fig. 4, we employ two non-Hermitian SSH chains as the two nodes. To satisfy the time-reversal requirements, we design the second non-Hermitian SSH chain to be a mirror image of the first one, with the two kinds of coupling parameters exchanged, i.e., $J_1^1 = J_2^2, J_2^1 = J_1^2$. By carefully selecting the dissipation strength, we can also ensure that the shape of the flying qubit is symmetric.

Here we provide two sets of parameters to achieve an ideal QST, where $N = 2$. In Fig. 5(a), the coupling strengths are selected as $J_1^1 = J_2^2 = J_0(1 - \cos(\omega t))$ and $J_2^1 = J_1^2 = J_0(1 + \cos(\omega t))$, respectively. Here, $J_0 = 5$ MHz is the coupling constant, and $\omega = 0.1$ MHz is the tuning frequency. The dissipation strength $\gamma_1 = \gamma_2 = \gamma = 0.6$ MHz at both nodes is constant. However, it is important to note that QST can still be achieved even when the coupling parameters do not satisfy the time-reversal relationship. In Fig. 5(b), the parameters we use are as follows: $J_1^1 = J_0 \sin(\omega t), J_2^1 = J_0 \cos(\omega t), J_2^2 = J_0(1 - \cos(\omega t)), J_1^2 = J_0(1 + \cos(\omega t)), J_0 = 5$ MHz, $\omega = 0.1$ MHz, $\gamma_1 = 0.6$ MHz, and $\gamma_2 = 0.23$ MHz. As shown in Figs. 5(a)
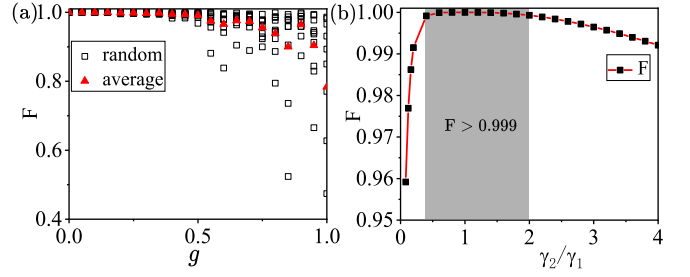

FIG. 6. (a) The fidelity of QST in the presence of errors in the coupling parameters. (b) With the dissipation strength at the first node fixed, the fidelity of the QST varies with different values of the dissipation strength at the second node. The dark shaded areas indicate ranges with fidelity greater than 0.999.

and 5(b), it is evident that by selecting suitable parameters, the quantum state initially located at node 1 can be transferred to node 2. Throughout the remainder of this paper, we will consistently employ the first set of parameters.

B. Fidelity of QST

In this section, we investigate the impact of imperfection factors on the fidelity of QST, including coupling parameter errors and imperfect chiral waveguides. In this paper, the fidelity of the QST, denoted as F, is defined as the overlap between the final state of node 2 and the ideal transfer state. The initial state of node 1 is

$$|\psi(t = 0)\rangle_1 = (|gg\cdots g\rangle_1 + |eg\cdots g\rangle_1)/\sqrt{2}. \quad (37)$$

The fidelity is

$$F = \left|{}_{\text{ideal}}\left\langle\psi\left(t = \frac{\pi}{\omega}\right)\middle|\psi\left(t = \frac{\pi}{\omega}\right)\right\rangle_2\right|, \quad (38)$$

where $|\psi(t = \frac{\pi}{\omega})\rangle_2$ is final state of node 2 at the end of the protocol and $|\psi(t = \frac{\pi}{\omega})\rangle_{\text{ideal}} = (|gg\cdots g\rangle_2 + e^{i\pi}|eg\cdots g\rangle_2)/\sqrt{2}$ is the final state of ideal QST. Here, the phase factor $e^{i\pi}$ is the adiabatic phase.

1. Parameter errors

In our protocol, errors in all coupling parameters of the chains can affect the QST. We consider the QST between two nodes, where the errors can be represented as follows:

$$\hat{H}_{\text{error}} = \sum_{j=1,2}\sum_n^N \left(\delta J_1^j \sigma_{A_{j,n}}^+ \sigma_{B_{j,n}}^- + \delta J_2^j \sigma_{B_{j,n}}^+ \sigma_{A_{j,n+1}}^-\right) + \text{H.c.} \quad (39)$$

As depicted in Fig. 6(a), we numerically simulate the effect of random errors in coupling parameters on fidelity, where the squares represent ten random simulations and the red triangles represent the average of ten simulations. The results demonstrate a significant plateau where high-fidelity QST can be achieved, indicating the robustness of our protocol in the presence of coupling parameter errors. This observation is in line with our expectations since the evolution of quantum states at the nodes occurs on topological edge states. Consequently, our protocol can maintain high-fidelity QST even in the presence of errors in the coupling parameters.
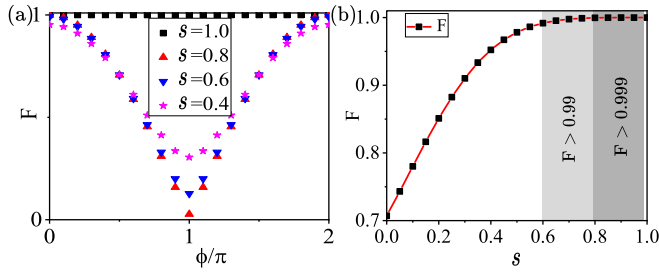
FIG. 7. (a) Fidelity as a function of the propagation phase ϕ for different s factors. The chirality rates s are $s = 1.0$ (black squares), $s = 0.8$ (red triangles), $s = 0.6$ (blue inverted triangles), and $s = 0.4$ (magenta stars). (b) The fidelity varies with the chirality rate with $\phi = 2n\pi$, where n is an integer.

The dissipation strength γ_j has an effect on the fidelity of the QST. In Fig. 6(b), we examine the effect of different dissipation strengths on the fidelity by fixing γ_1 at node 1 and varying γ_2 at node 2. The results show that the fidelity of QST exceeds 0.999 when γ_2 is within the range $[0.5\gamma_1, 2\gamma_1]$, demonstrating the robustness of our protocol in the presence of dissipation strength errors.

2. Imperfect chirality

In all of the previous descriptions, we assume perfect chiral waveguides where the nodes are only coupled to the right-moving modes. Now, we extend our analysis to include the coupling between the nodes and the left-moving modes of the waveguide. In this case, the interaction Hamiltonian between the two nodes and the waveguide can be described as follows:

$$
\hat{H}_I = i \sum_{j=1,2} \sqrt{2s\gamma_j} c_R^\dagger(t - (j-1)\tau) e^{i(j-1)\phi_R} \sigma_{A_{j,N+1}}^-
$$
$$
+ i \sum_{j=1,2} \sqrt{2(1-s)\gamma_j} c_L^\dagger(t + (j-1)\tau) e^{-i(j-1)\phi_L} \sigma_{A_{j,N+1}}^-
$$
$$
- \text{H.c.}, \tag{40}
$$

where s is the chirality rate; $s\gamma_j$ and $(1-s)\gamma_j$ represent the coupling strengths between the nodes and waveguide for the right-moving mode and left-moving mode, respectively. The

propagation phase $\phi = \phi_R = \phi_L$ and time delay τ will affect the fidelity of the QST.

To ensure the validity of the Markovian assumption in our protocol, we assume that the time delay between two nodes is much larger than the evolution time of the system, i.e., $\gamma\tau \ll 1$. As illustrated in Fig. 7(a), we describe the effect of the propagation phase on the fidelity of QST. When the channel is a perfect chiral waveguide, the fidelity remains unaffected by changes in the propagation phase. However, for other values of s, high-fidelity QST can only be achieved when the propagation phase is $\phi = 2n\pi$, indicating that the distance between the two nodes is an integer multiple of the wavelength. In Fig. 7(b), we fix the distance between the two nodes to be an integer multiple of the wavelength. It is evident that when the chirality rate is greater than 0.6, the fidelity of QST exceeds 0.99. Moreover, for chirality rates greater than 0.8, the fidelity is even higher, surpassing 0.999.

IV. CONCLUSION

In conclusion, we have proposed a robust QST protocol that takes non-Hermitian SSH chains as the nodes in quantum networks. By analyzing the symmetry and dynamic properties of a single node, we have demonstrated that the edge mode in the non-Hermitian SSH chain has an imaginary spectrum. The topological edge mode can be used to encode (decode) the quantum state (flying qubit), which remains unaffected by coupling imperfections. Numerical simulations show that ideal QST can be achieved between distant nodes, even in the presence of significant coupling parameter errors. Furthermore, we have observed high-fidelity QST at a high chirality rate when the distance between nodes is an integer multiple of the wavelength. This protocol introduces an alternative approach to constructing quantum networks and can be implemented on various physical platforms.

[1] H. J. Kimble, Nature (London) **453**, 1023 (2008).

[2] A. Reiserer and G. Rempe, Rev. Mod. Phys. **87**, 1379 (2015).

[3] T. E. Northup and R. Blatt, Nat. Photonics **8**, 356 (2014).

[4] J. I. Cirac, P. Zoller, H. J. Kimble, and H. Mabuchi, Phys. Rev. Lett. **78**, 3221 (1997).

[5] T. Pellizzari, Phys. Rev. Lett. **79**, 5242 (1997).

[6] D. N. Matsukevich and A. Kuzmich, Science **306**, 663 (2004).

[7] K. Stannigel, P. Rabl, A. S. Sørensen, P. Zoller, and M. D. Lukin, Phys. Rev. Lett. **105**, 220501 (2010).

[8] K. Stannigel, P. Rabl, A. S. Sørensen, M. D. Lukin, and P. Zoller, Phys. Rev. A **84**, 042341 (2011).

[9] T. Ramos, B. Vermersch, P. Hauke, H. Pichler, and P. Zoller, Phys. Rev. A **93**, 062104 (2016).

[10] S. Bose, Phys. Rev. Lett. **91**, 207901 (2003).

[11] M. Christandl, N. Datta, A. Ekert, and A. J. Landahl, Phys. Rev. Lett. **92**, 187902 (2004).

[12] F. Mei, G. Chen, L. Tian, S.-L. Zhu, and S. Jia, Phys. Rev. A **98**, 012331 (2018).

[13] Y. Li, J. Zhang, Y. Wang, H. Du, J. Wu, W. Liu, F. Mei, J. Ma, L. Xiao, and S. Jia, Light Sci. Appl. **11**, 13 (2022).

[14] Y. Wang, J.-H. Zhang, Y. Li, J. Wu, W. Liu, F. Mei, Y. Hu, L. Xiao, J. Ma, C. Chin, and S. Jia, Phys. Rev. Lett. **129**, 103401 (2022).

[15] P. Lodahl, S. Mahmoodian, S. Stobbe, A. Rauschenbeutel, P. Schneewiss, J. Volz, H. Pichler, and P. Zoller, Nature (London) **541**, 473 (2017).

[16] R. Mitsch, C. Sayrin, B. Albrecht, P. Schneeweiss, and A. Rauschenbeutel, Nat. Commun. **5**, 5713 (2014).

[17] I. Söllner, S. Mahmoodian, S. L. Hansen, L. Midolo, A. Javadi, G. Kiršanskė, T. Pregnolato, H. El-Ella, E. H. Lee, J. D. Song, S. Stobbe, and P. Lodahl, Nat. Nanotechnol. **10**, 775 (2015).

[18] S. Ritter, C. Nölleke, C. Hahn, A. Reiserer, A. Neuzner, M. Uphoff, M. Mücke, E. Figueroa, J. Bochmann, and G. Rempe, Nature (London) **484**, 195 (2012).

[19] C. Eichler, C. Lang, J. M. Fink, J. Govenius, S. Filipp, and A. Wallraff, Phys. Rev. Lett. **109**, 240501 (2012).

[20] A. F. van Loo, A. Fedorov, K. Lalumière, B. C. Sanders, A. Blais, and A. Wallraff, Science **342**, 1494 (2013).

[21] N. Y. Yao, L. Jiang, A. V. Gorshkov, Z.-X. Gong, A. Zhai, L.-M. Duan, and M. D. Lukin, Phys. Rev. Lett. **106**, 040505 (2011).

[22] S. Bose, Contemp. Phys. **48**, 13 (2007).

[23] Z. Song and C. P. Sun, Low Temp. Phys. **31**, 686 (2005).

[24] M. Z. Hasan and C. L. Kane, Rev. Mod. Phys. **82**, 3045 (2010).

[25] X.-L. Qi and S.-C. Zhang, Rev. Mod. Phys. **83**, 1057 (2011).

[26] T. Ozawa, H. M. Price, A. Amo, N. Goldman, M. Hafezi, L. Lu, M. C. Rechtsman, D. Schuster, J. Simon, O. Zilberberg, and I. Carusotto, Rev. Mod. Phys. **91**, 015006 (2019).

[27] L. A. Wray, S.-Y. Xu, Y. Xia, D. Hsieh, A. V. Fedorov, Y. S. Hor, R. J. Cava, A. Bansil, H. Lin, and M. Z. Hasan, Nat. Phys. **7**, 32 (2011).

[28] M. Malki and G. S. Uhrig, Phys. Rev. B **95**, 235118 (2017).

[29] C. Xu and J. E. Moore, Phys. Rev. B **73**, 045322 (2006).

[30] V. Peano, C. Brendel, M. Schmidt, and F. Marquardt, Phys. Rev. X **5**, 031011 (2015).

[31] H. Zhu, J. Yi, M.-Y. Li, J. Xiao, L. Zhang, C.-W. Yang, R. A. Kaindl, L.-J. Li, Y. Wang, and X. Zhang, Science **359**, 579 (2018).

[32] N. R. Bernier, L. D. Toth, A. Koottandavida, M. A. Ioannou, D. Malz, A. Nunnenkamp, A. Feofanov, and T. Kippenberg, Nat. Commun. **8**, 604 (2017).

[33] J. Niu, T. Yan, Y. Zhou, Z. Tao, X. Li, W. Liu, L. Zhang, H. Jia, S. Liu, Z. Yan, Y. Chen, and D. Yu, Sci. Bull. **66**, 1168 (2021).

[34] Y. Wang, H. Du, Y. Li, F. Mei, Y. Hu, L. Xiao, J. Ma, and S. Jia, Light Sci. Appl. **12**, 50 (2023).

[35] C. Nayak, S. H. Simon, A. Stern, M. Freedman, and S. Das Sarma, Rev. Mod. Phys. **80**, 1083 (2008).

[36] W. M. Witzel and S. Das Sarma, Phys. Rev. B **74**, 035322 (2006).

[37] M. Parto, S. Wittek, H. Hodaei, G. Harari, M. A. Bandres, J. Ren, M. C. Rechtsman, M. Segev, D. N. Christodoulides, and M. Khajavikhan, Phys. Rev. Lett. **120**, 113901 (2018).

[38] Z.-Q. Yang, Z.-K. Shao, H.-Z. Chen, X.-R. Mao, and R.-M. Ma, Phys. Rev. Lett. **125**, 013903 (2020).

[39] Y. V. Kartashov and D. V. Skryabin, Phys. Rev. Lett. **122**, 083902 (2019).

[40] C. Dlaska, B. Vermersch, and P. Zoller, Quantum Sci. Technol. **2**, 015001 (2017).

[41] C. Wang, L. Li, J. Gong, and Y.-X. Liu, Phys. Rev. A **106**, 052411 (2022).

[42] L.-N. Zheng, L. Qi, L.-Y. Cheng, H.-F. Wang, and S. Zhang, Phys. Rev. A **102**, 012606 (2020).

[43] F. M. D'Angelis, F. A. Pinheiro, D. Guéry-Odelin, S. Longhi, and F. Impens, Phys. Rev. Res. **2**, 033475 (2020).

[44] N. E. Palaiodimopoulos, I. Brouzos, F. K. Diakonos, and G. Theocharis, Phys. Rev. A **103**, 052409 (2021).

[45] Z. Gong, Y. Ashida, K. Kawabata, K. Takasan, S. Higashikawa, and M. Ueda, Phys. Rev. X **8**, 031079 (2018).

[46] K. Kawabata, K. Shiozaki, M. Ueda, and M. Sato, Phys. Rev. X **9**, 041015 (2019).

[47] J. R. Johansson, P. D. Nation, and F. Nori, Comput. Phys. Commun. **184**, 1234 (2013).

[48] J. R. Johansson, P. D. Nation, and F. Nori, Comput. Phys. Commun. **183**, 1760 (2012).